E&G Quaternary Sci. J., 71, 91–110, 2022
https://doi.org/10.5194/egqsj-71-91-2022

Open Access E&G Quaternary Science Journal

Research article

Holocene vegetation reconstruction in the forest–steppe of Mongolia based on leaf waxes and macro-charcoals in soils

Marcel Lerch[1], **Julia Unkelbach**[2], **Florian Schneider**[3], **Michael Zech**[1], **and Michael Klinge**[3]

[1]Heisenberg Chair of Physical Geography with Focus on Paleoenvironmental Research, Institute of Geography, Technische Universität Dresden, Helmholtzstraße 10, 01069 Dresden, Germany
[2]Department of Palynology and Climate Dynamics, Albrecht-von-Haller-Institute for Plant Sciences, University of Göttingen, Untere Karspüle 2, 37073 Göttingen, Germany
[3]Department of Physical Geography, Institute of Geography, University of Göttingen, Goldschmidtstr. 5, 37077 Göttingen, Germany

Correspondence: Michael Klinge (mklinge1@gwdg.de)

Relevant dates: Received: 25 October 2021 – Revised: 20 March 2022 – Accepted: 2 May 2022 – Published: 24 May 2022

How to cite: Lerch, M., Unkelbach, J., Schneider, F., Zech, M., and Klinge, M.: Holocene vegetation reconstruction in the forest–steppe of Mongolia based on leaf waxes and macro-charcoals in soils, E&G Quaternary Sci. J., 71, 91–110, https://doi.org/10.5194/egqsj-71-91-2022, 2022.

Abstract: Vegetation and climate reconstruction in the forest–steppe of Mongolia is still challenging regarding the pattern of forest and grassland distribution during the Holocene. Different sediments containing paleosols and humic layers provide geomorphological archives for landscape development in Mongolia. *n*-Alkane and macro-charcoal ratios represent specific indicators to distinguish the share between grasses and trees. In a preliminary study, we investigated the applicability of these two paleo-proxies from soils for vegetation reconstruction comparing different relief positions and site conditions in the northern Khangai Mountains of Mongolia.

n-Alkanes that are deposited from leaf waxes in the soil have the potential to indicate vegetation composition on a local scale. Depending on site-specific environmental conditions, *n*-alkanes are subjected to different degrees of microbiological decomposition, which is more intensive in soils of dry steppe than of forests. Mongolian forests are often underlain by permafrost that may reduce microbiological activity. In steppe soils, the decomposition of *n*-alkanes increases the quantity of mid-chain *n*-alkanes that adulterate the biomarker proxy signal to indicate more forest share. Macro-charcoals in soils have a site-specific component, but additional eolian input of macro-charcoals from long-distance transport can provide a distinct proportion in sediments. Thus, eolian influx of wood-derived macro-charcoal can dominate the proxy signal at sites where trees were few or had never existed.

Radiometric dating of several paleosols and humic layers has shown that both proxies coincide as evidence for high grassland-to-forest ratios during the Early Holocene. By contrast, the proxy signals diverge for the Late Holocene. For this period, *n*-alkanes generally indicate more grassland, whereas macro-charcoals show increased wood-derived proportions. We imply that this difference is caused by increased forest fires and simultaneously spreading steppe area.

Published by Copernicus Publications on behalf of the Deutsche Quartärvereinigung (DEUQUA) e.V.

A main portion of leaf waxes and charcoal particles in soils directly derive from the covering and nearby vegetation, whereas large lakes and glacier may receive these biomarkers from a larger catchment area. Thus, we conclude that soil archives provide proxies on a more local and site-specific scale than other archives do. Although the temporal resolution of soil archives is lower than for the other ones, biomarker proxies for paleosols and humic layer can be related to periods of distinct geomorphological processes. Further investigations comparing the multi-proxy data of different geomorphological archives are necessary to improve the paleo-ecological reconstruction for landscape development in Mongolia.

Kurzfassung:

Die Rekonstruktion von Klima und Vegetation in der mongolischen Waldsteppe stellt nach wie vor eine große Herausforderung in Hinsicht auf die Verbreitungsmuster von Wald- und Grasslandschaften im Laufe des Holozäns dar. Verschiedenartige Sedimente mit Paläoböden und organischen Schichten können dafür als hervorragende Archive für die Analyse der Landschaftsentwicklung in der Mongolei dienen. Die proportionalen Verhältnisse verschiedener *n*-Alkane und Typen von Holzkohlepartikeln lassen sich als Indikatoren zur Bestimmung der Grass und Baumanteile heranziehen. Im Rahmen einer Vorstudie haben wir die Anwendbarkeit dieser zwei Paläoproxies für die Vegetationsrekonstruktion aus Bodenarchiven untersucht. Dafür wurden Profile mit unterschiedlichen Reliefpositionen und Standortbedingungen aus einem Untersuchungsgebiet im Norden des Khangai-Gebirges in der Mongolei verglichen.

n-Alkane von der Wachsschicht der Blätteroberflächen gelangen in den Boden und bieten die Möglichkeit die Zusammensetzung der Vegetation auf lokaler Ebene zu analysieren. Abhängig von den standortspezifischen Umweltbedingungen werden *n*-Alkane mikrobiell unterschiedlich stark abgebaut, wobei der Abbau in Böden der Trockensteppen intensiver ist als in den Wäldern. In den Wäldern der Mongolei ist häufig Permafrost im Boden vorhanden, der die mikrobiologische Aktivität verringert. In den Steppenböden erhöht sich durch die Zersetzung von *n*-Alkanen den Anteil an mittelkettigen *n*-Alkanen, was das Biomarker-Proxysignal in Richtung eines höheren Waldanteils verfälscht. Holzkohlepartikel in Böden haben eine standortspezifische Komponente. Allerdings kann ein zusätzlicher äolischer Eintrag von Holzkohlepartikeln aus dem Ferntransport einen deutlichen Anteil in den Sedimenten ausmachen. Durch den äolischen Anteil können holzspezifische Kohlepartikel in den Proxysignalen an Standorten dominieren, an denen es nur wenige oder niemals Bäume gab.

Radiometrische Datierungen von Paläoböden und organischen Schichten zeigen, dass beide Proxys einen hohen Anteil von Grasland gegenüber Wald im frühen Holozän aufweisen. Im Gegensatz dazu divergieren die Proxysignale für das späte Holozän. Für diesen Zeitraum deuten *n*-Alkane allgemein auf mehr Grasland hin, während die Holzkohlepartikel einen höheren Waldanteil erkennen lassen. Wir vermuten, dass dieser Unterschied durch vermehrte Waldbrände und die gleichzeitige Ausbreitung von Steppenflächen verursacht wurde.

Allgemein lässt sich folgern, dass Bodenarchive mehr lokale und ortsspezifische Proxies liefern als es bei Archiven aus Seen und Gletschereis zu erwarten ist. Diese Archive erhalten einen Materialeintrag aus wesentlich größeren Einzugsgebieten. Obwohl die zeitliche Auflösung von Bodenarchiven geringer ist als bei den anderen Archiven, können Biomarker aus Paläoböden und humosen Schichten mit Perioden spezifischer geomorphologischer Prozesse verknüpft werden. Weitere Detailuntersuchungen zum Vergleich von Multiproxy-Daten aus verschiedenen geomorphologischen Archiven sind notwendig, um die paläoökologischen Rekonstruktionen zur Landschaftsentwicklung in der Mongolei auf regionaler Ebene zu verbessern.

1 Introduction

The Mongolian forest–steppe represents a zonal ecotone at the southern fringe of the Siberian boreal forests (Breckle et al., 2002; Erdős et al., 2018). Due to the continental and semi-arid climate, the vegetation pattern of forest patches and open grassland is controlled by local geo-ecological conditions (Dulamsuren and Hauck, 2008; Hais et al., 2016; Khansaritoreh et al., 2017). Paleo-environmental reconstruction based on vegetation distribution is the key for interpreting climate and human impact on the Holocene landscape development.

Pollen analyses are most commonly used to produce proxy data for paleo-vegetation. Peat bogs and lake sediments represent efficient archives for pollen analysis that can provide long-term and high-resolution paleo-environmental records (Fowell et al., 2003; Rudaya et al., 2009; Unkelbach et al., 2021). However, the pollen influx depends on near- and long-distance transport and plant-specific pollen productivity. Thus, pollen spectra represent a mixture of different vegetation types from a wide catchment area (Odgaard, 1999; Zech et al., 2010b). Pollen analyses from soil material may be hampered by selective pollen decomposition under aerobic conditions. In contrast, charcoal particles from burned vegetation and long-chain *n*-alkanes originating from leaf waxes (Eglinton and Hamilton, 1967; Kolattukudy, 1976) are relatively resistant against physical, chemical and biological degradation. The long-lasting persistence of charcoal and long-chain *n*-alkanes in soil provides a valuable archive tool for reconstruction of local paleo-vegetation (Patterson et al., 1987; Bliedtner et al., 2020; Thomas et al., 2021).

Few investigations on charcoal and *n*-alkane distribution exist for different paleo-environmental archives in Mongolia and central Asia. Charcoal records from Mongolia have been reported from lacustrine archives (Umbanhowar et al., 2009; Unkelbach et al., 2019, 2021) and glaciers (Brugger et al., 2018). These records have predominantly been used for the reconstruction of fire chronologies. Furthermore, Miehe et al. (2007) found charcoal pieces from birch, willow and coniferous trees in soils of the Gobi Altai Mountains as evidence for forest distribution in southern Mongolia before 4 ka. In addition to charcoal, long-chain *n*-alkane patterns and ratios were used for the reconstruction of past vegetation composition (Zech et al., 2010b; Tarasov et al., 2013). In a case study along several transects in Mongolia, Struck et al. (2020) have shown that the total *n*-alkane concentration (TAC) and the odd-over-even predominance (OEP) from topsoils significantly correlate with climate parameters. OEP and TAC increase with low temperatures and high precipitation. The authors explain low *n*-alkane concentrations in topsoils by low biomass production, enhanced alkane degradation and livestock grazing intensity. Furthermore, Struck et al. (2020) found no climate effect on the average chain length (ACL) and the *n*-alkane ratio ($n\mathrm{C}_{31}/(n\mathrm{C}_{29}+n\mathrm{C}_{31})$) of plants and topsoils. Thus, the authors proposed the applicability of these indices to distinguish between vegetation dominated by grasses and woody shrubs.

According to literature data, vegetation composition consisting of deciduous trees and shrubs is characterized by dominant *n*-alkane chain lengths of $n\mathrm{C}_{27}$ and $n\mathrm{C}_{29}$, whereas grasses and herbs show dominant *n*-alkane chain lengths of $n\mathrm{C}_{31}$ and $n\mathrm{C}_{33}$ (Zech et al., 2010a, b; Schäfer et al., 2016). Apart from leaf waxes, charred biomass and soil, microbial biomass may also contribute to the *n*-alkane fractions in paleosols (Zech et al., 2017). Wiesenberg et al. (2009) investigated the thermal degradation of rye and maize straw and found that short-chain *n*-alkanes in soils may serve as a marker for charred grass biomass. Hence, Zech et al. (2017), who evaluated post-depositional contamination of *n*-alkane biomarkers in paleosols, interpreted $n\mathrm{C}_{18}$ as a proxy for charred sedimentary organic matter. In addition, decomposition by soil microorganisms generates short- and mid-chain *n*-alkanes (Buggle et al., 2010; Zech et al., 2017). In semi-arid regions of central Asia, different relief positions and topographic asymmetries in soil moisture and vegetation cover induce specific variations in soil ecological conditions (Iijima et al., 2012; Kopp et al., 2014; Hais et al., 2016; Pelletier et al., 2018) and control the distribution of discontinuous permafrost (Klinge et al., 2021). The differing geo-ecological conditions lead to differences in the soil formation rate and microbiological activity. Thus, the degree of *n*-alkane decomposition varies between different topographic sites and soil conditions that may influence effectively the *n*-alkane pattern and its relevance for paleo-environmental interpretation in terms of paleo-vegetation.

Geomorphological mapping and investigation of soil profiles for reconstruction of Holocene landscape development comprise a general aim of the research project (Klinge et al., 2022). As part of the general aim, we intended to evaluate the applicability of macro-charcoal and *n*-alkanes for reconstruction of past vegetation composition from paleosols and humic layers in the semi-arid forest-steppe region of Mongolia by executing two different approaches for proxy-data analysis. We calculated macro-charcoal and *n*-alkane ratios for data interpretation. Furthermore, we evaluated mid-chain *n*-alkane contents related to soil properties to estimate microbiological activity and biomass decomposition in humic layers and paleosols and distinguish their paleo-environmental relevance between different site conditions.

2 Material and methods

2.1 Study area

The study area is located near the town of Tosontsengel (48°46′ N, 98°16′ E; 1670 m a.s.l.) in the northern Khangai Mountains of central Mongolia (Fig. 1). At Tosontsengel, the mean monthly temperatures range between −31.7 °C in January and 14.7 °C in July (National Agency for Meteorology and Environment Monitoring of Mongolia, Ulaanbaatar).

The annual precipitation amounts to 220 mm and reaches up to 500 mm in higher altitudes (Academy of Sciences of Mongolia and Academy of Sciences of USSR, 1990). Most of the precipitation occurs in summer during the growing season, whereas winters are mostly dry. Forest–steppe is the dominating vegetation under the continental and semi-arid climate. Cold conditions lead to the distribution of discontinuous permafrost. Permafrost mainly occurs in valley bottoms, on upper mountains and partially on north-facing slopes under large forest stands (Klinge et al., 2021). In the central Khangai Mountains in the south, the mountains reach up to 3200 m a.s.l., whereas the main river in the north, the Ider Gol, is situated around 1600 m a.s.l. The upper treeline rises southward from 2400 to 2600 m a.s.l., while a lower treeline occurs at around 1800 m a.s.l. (Klinge et al., 2018).

Fragmented forests with Siberian larch (*Larix sibirica*) are generally limited to north-facing slopes. Steppe vegetation covers south-facing slopes and the pediments in the basins (*Artemisia* spp., Chenopodiaceae, Poaceae, *Potentilla fruticosa*). Steppe-like grass vegetation spreads into small forest patches and open forest fringes, whereas the ground vegetation of large forests mostly consists of mosses, herbs and shrubs (*Lonicera altaica*, *Vaccinium vitis-idaea*, *Vaccinium myrtillus*). Large forest stands are often accompanied by a belt of broadleaf trees and bushes (*Salix* spp., *Betula* spp.) at toe slopes and in slope depressions, where increased soil moisture is available. Along the rivers, riparian woody vegetation including willow (*Salix* spp.), poplar (*Populus* spp.) and larch (*Larix sibirica*) occurs. The semi-arid conditions promote frequent forest fires in this region, which occur simultaneously with droughts and are often caused by human fire setting (Nyamjav et al., 2007; Hessl et al., 2016). Due to these conditions, tree regrowth on burned sites strongly depends on soil hydrological properties and occurs irregularly (Schneider et al., 2021). Forest distribution in the study area since 9.5 ka has been shown by Unkelbach et al. (2021), and fire intensity increased after 4.5 ka (Klinge et al., 2022). *Epilobium angustifolium* is a common fire indicator that spreads in burned forests (Khapugin et al., 2016).

2.2 Soil sampling and dating

Sampling of soil and vegetation was carried out during fieldwork in Mongolia in the summers of 2018 and 2019. We took sediment samples from 12 soil profiles for analyses. Organic matter from paleosols and humic layers was used for ^{14}C dating, whereas intermediate eolian layers were analyzed by infrared stimulated luminescence (IRSL) dating. Details on dating methods and soil properties and results for geomorphological processes were published by Klinge et al. (2022). All ^{14}C ages are given as calibrated ^{14}C ages in thousands of years before present (ka BP) here. Samples for biomarker and charcoal analyses were taken parallel to soil samples by a separate sampling procedure.

2.3 Sample preparation and element analyses

Analyses of leaf-wax-derived *n*-alkanes were carried out on 35 soil samples and 6 modern vegetation samples that were collected at the study site. *n*-Alkane analyses as well as total carbon and total nitrogen measurements were executed at the laboratory facilities of the Department of Soil Biogeochemistry, Institute of Agricultural and Nutritional Sciences, Martin Luther University Halle-Wittenberg, in Halle (Saale). Soil samples were air-dried and sieved (< 2 mm) for preparation. Vegetation samples were dried, and whole leaves were used for analysis.

The contents of total carbon (TC) and total nitrogen (TN) were measured using a EuroVector EA3000 elemental analyzer (Hekatech, Wegberg, Germany) coupled via a Conflow III interface to a Delta V Advantage isotope ratio mass spectrometer (Thermo Fisher Scientific, Bremen, Germany).

2.4 Lipid biomarker analyses

n-Alkane preparation and quantification followed the procedure described by, e.g., Lerch et al. (2018) and Zech et al. (2013). In brief, the total lipid extracts (TLEs) of all soil and modern vegetation samples were gained using Soxhlet extraction in 24 h and of $\sim$ 180 mL dichloromethane (DCM) : methanol (MeOH) (9 : 1) as the solvent mixture. The necessary sample amount for *n*-alkane analysis depends on the total organic carbon content (TOC). The sample weight for the investigated soil material ranged from $\sim$ 3 to 8 g. A sample weight of $\sim$ 1 g was chosen for plant material, and 5α-androstane was added as an internal standard to each vegetation and soil sample. Additionally, we inserted $\sim$ 1 g of glass wool into extraction thimbles for prevention of the splash effect before extraction started. Afterwards, the TLE was dried with a rotary evaporator and dissolved again with *n*-hexane. For separation of the TLE, aminopropyl silica gel (45 µm; Supelco) pipette columns were used (Struck et al., 2018). The dissolved TLE was separated as well as eluted over these pipette columns into (i) an aliphatic fraction (apolar) including the *n*-alkanes using *n*-hexane (3 × 1 mL), (ii) an alcoholic fraction (polar) using DCM : MeOH (9 : 1, 3 × 1 mL) and (iii) an acid fraction using diethyl ether : acetic acid (95 : 5, 3 × 1 mL) for each sample. Afterwards, separated fractions were dried under nitrogen. The aliphatic fraction was transferred into 1.5 mL gas chromatography vials with 2 × 0.5 mL *n*-hexane for measurements. *n*-Alkanes were identified and quantified with a gas chromatograph coupled with a flame ionization detector (GC-FID, 2010 series, Shimadzu, Kyoto, Japan). External *n*-alkane standards with a known concentration (*n*-alkane mix nC_8–nC_{40}; Supelco 49452-U) were repeatedly run with each sequence at different concentrations (25, 50 and 100 µg mL^{-1}) for quantification and identification (Hepp et al., 2017; Bliedtner et al., 2018; Bittner et al., 2020). Detailed results of *n*-alkane analysis are shown in Table S2 in the Supplement.

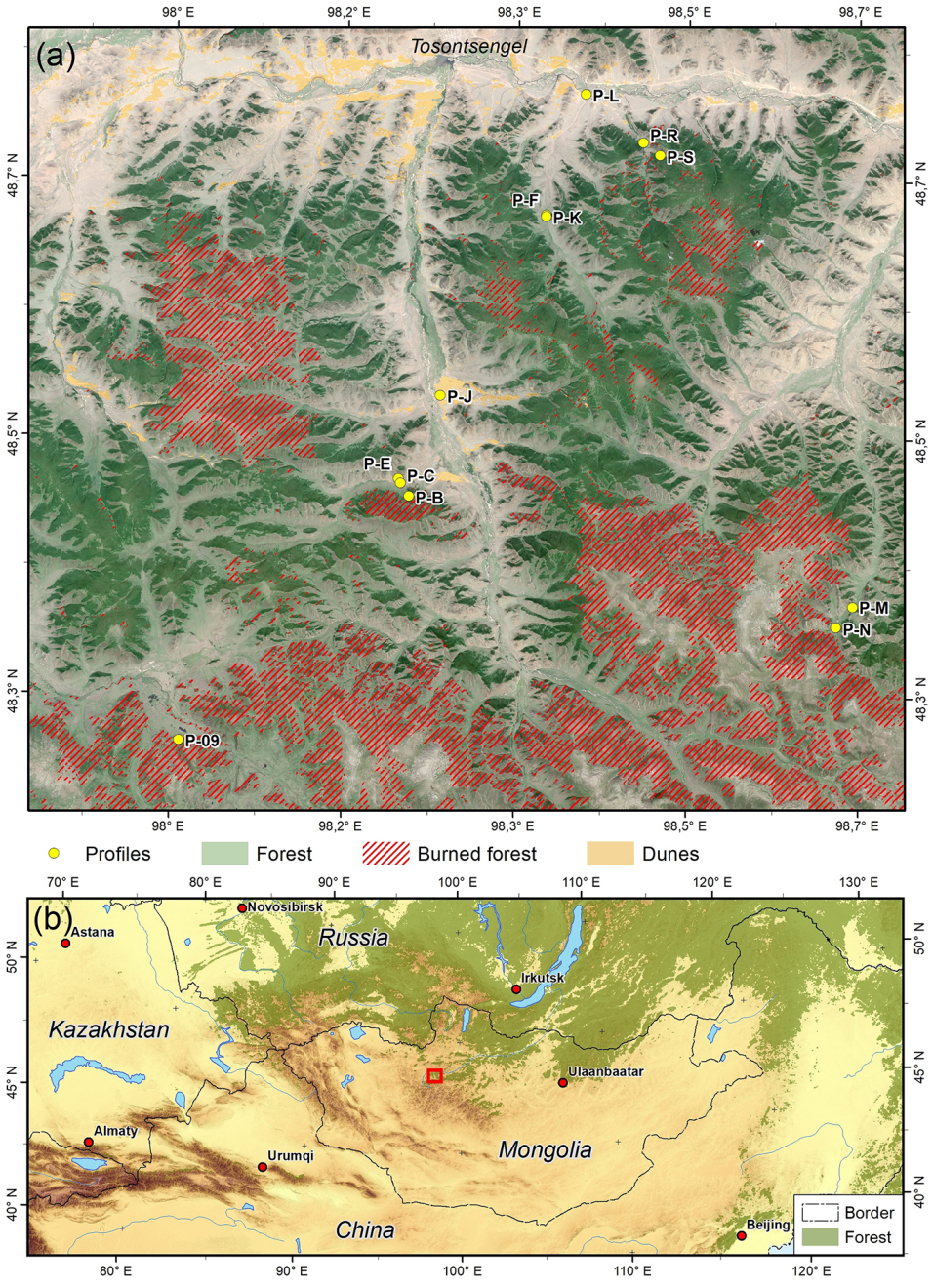

Figure 1. **(a)** Study area and sample sites. The shaded relief is based on TanDEM-X data (© DLR 2011), and the background image is based on Copernicus Sentinel data (31 July 2019). **(b)** Regional overview with red rectangle indicating the position of the study area.

2.5 Macro-charcoal analysis

For macro-charcoal analysis, 27 subsamples of 0.5 cm^3 were taken from organic layers and paleosols. All subsamples were processed based on the method established by Stevenson and Haberle (2005), including KOH (10 %), H_2O_2 (4 %) and wet sieving with low water pressure to avoid further fragmentation of the charcoal material. All charred macroparticles (> 125 µm) of each subsample were counted using a binocular dissecting microscope. To reconstruct dominating vegetation types (forest, steppe), all charred particles were divided into four different morphological types while counting: wood (rather 3-dimensional, long), leaf (rather 2-dimensional, irregularly shaped), grass (rather 2-dimensional, long and mostly rectangular) and other (including mosses, roots, seeds and unidentifiably small fragments). Macro-charcoal identification was based on the examples given in Umbanhowar and Mcgrath (1998) and Mustaphi and

Pisaric (2014). Additionally, macro-charcoal concentrations (particle sum per cubic centimeter) were calculated for each subsample (Supplement File S1).

2.6 Data analysis

Macro-charcoals were classified as originating from wood, leaf and grass. Approx. 25 % of particles could not be identified or had another source and were classified as other and excluded from statistical analysis. The share of charcoal classes was determined to evaluate steppe / forest ratios (C_{sf}) that could indicate vegetation composition:

$$C_{sf} = \frac{\text{grass}}{\text{wood}}. \quad (1)$$

The OEP (odd-over-even predominance) ratio considers long-chain *n*-alkanes and can be used as proxy for *n*-alkane degradation (Zech et al., 2012). High OEP values correspond to fresh plant material, whereas lower OEP values indicate an increased degradation of soil organic matter (Schäfer et al., 2016).

$$\text{OEP} = \frac{nC_{27} + nC_{29} + nC_{31} + nC_{33}}{nC_{26} + nC_{28} + nC_{30} + nC_{32}}, \quad (2)$$

defined as odd-over-even predominance (OEP) according to Hoefs et al. (2002).

The C / N ratio serves as an additional soil parameter for biological decomposition.

Based on *n*-alkane patterns of the analyzed vegetation samples and their dominant *n*-alkane chain lengths, calculated *n*-alkane proxy data can be applied for soils regarding vegetation reconstruction (Zech et al., 2012). Here, we used the ACL (Poynter et al., 1989), defined as the average chain length of *n*-alkanes, in the modified version reported from Schäfer et al. (2016) to address the grassland–woodland composition:

$$\text{ACL} = \frac{27 \times nC_{27} + 29 \times nC_{29} + 31 \times nC_{31} + 33 \times nC_{33}}{nC_{27} + nC_{29} + nC_{31} + nC_{33}}. \quad (3)$$

To indicate fire marker and soil microbial degradation, we checked the short-chain *n*-alkane fraction by elevated values of nC_{18} and $\sum nC_{17}$–nC_{20} to be compared with OEP, C / N and macro-charcoal distribution. Elevated nC_{18} contents along with higher OEP and C / N ratios indicate an input of charred biomass.

The relationship between charcoal and *n*-alkane parameters was assessed by producing bivariate scatterplots and performing a series of correlation analyses. Each relationship was assessed based on correlation coefficients (Pearson's *r*) with a significance threshold (*p* value) set at 0.5.

3 Results and discussion

3.1 Soil profiles and dating results

Paleosols and humic layers containing abundant charcoal were found in various soil profiles in topographic positions on slopes under forest and steppe, dunes, and alluvial plains (Fig. 1). Figure 2 illustrates the soil profiles with positions of samples for soil analyses and dating, which are described in detail in the following section. We classified the soil profiles into three site groups. Group A contains all sites where trees exist or have existed before. Group B comprises sites of exclusively steppe vegetation. All sites with inconsistent dating results and where a mixture of different solum material was found were assigned to group C, which represents problematic profiles for correlation analyses.

Profile P-B (Fig. 2, group A) was located in a toe-slope position inside a dense larch succession at a formerly burned forest site. The profile was composed of colluvial sediments with an imbricated layering that derived from downslope transport of solum after repeated forest fires (Klinge et al., 2021). The solum material was rich in soil organic matter (SOM), and ^{14}C dating of charcoal from different layers provided upward consistent calibrated ^{14}C ages of between 3.8 and 2.0 ka. This dating indicates the ages of the trees that burned in an upslope position during distinct fire events. Two IRSL ages at around 10 ka from intermediate yellowish sand layers pointed to the time of primary eolian deposition further upslope before this sand was transported downslope by colluvial and/or periglacial processes that occurred after 3.3 ka (Klinge et al., 2022). Permafrost occurred at a depth of > 90 cm. Soil profile P-S (Fig. 2, group C) was located at a valley bottom under dense broadleaf vegetation (*Betula*, *Salix*). Intensively cryoturbated colluvial and eolian sediments with paleosols, humic layers and charcoal were found, and permafrost ice occurred at a depth of 70 cm. Carbon-14 dating of charred material and SOM provided calibrated ages of between 2.7 and 0.45 ka, whereas eolian material yielded an IRSL age of 12.1 ka. The time–depth inconsistency of the ages may be due to colluvial, cryoturbation and solifluction processes (Klinge et al., 2022).

Section P-C (Fig. 2, group B) was exposed in a gully in a basin under steppe vegetation. The sediment consisted of two units. The lower unit rested on Pleistocene fanglomerates and was composed of homogeneous eolian sand which provided IRSL ages of between 11.0 and 8.9 ka. Two ^{14}C dating analyses of SOM from a distinct paleosol upon the lower sediment unit provided calibrated ages of 1.8 ± 0.1 and 0.9 ± 0.1 ka, whereas IRSL dating from the upper sediment obtained an age of 1.1 ka (Klinge et al., 2022). In the transition to the upper sediment unit, the paleosol layers diverged into several sub-units, where a humpy upper boundary pointed to enhanced dust trapping around tussock grass. The 60 cm thick upper sediment unit above the paleosol consisted of layered sediments that derived from repeated slope wash processes. A conspicuous black layer at 6 cm depth contained abundant charcoal. Section P-R (Fig. 2, group A) was located at an alluvial fan under steppe vegetation adjacent to an alluvial forest. The sediments consisted of colluvial and slope wash layers including three paleosols with charcoal and several dark brown humic layers. Carbon-14 dating of SOM pro-

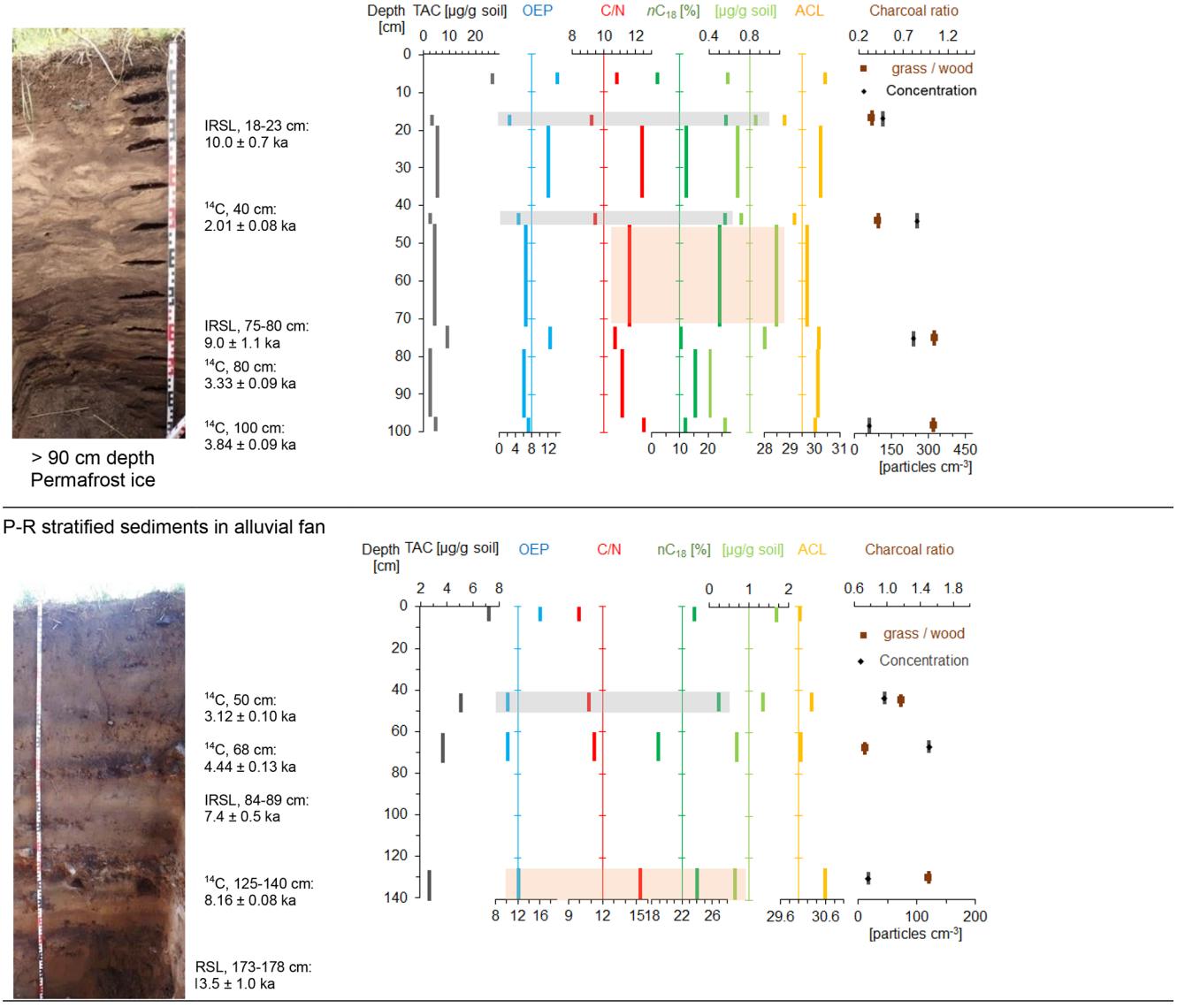

Figure 2.

vided time–depth-consistent calibrated ages of 3.1, 4.4 and 8.2 ka, which were complemented by two IRSL ages of 7.4 and 13.5 ka. In contrast to the profiles P-B and P-S that were located under forest, no permafrost was found at sections P-C and P-R under steppe. This difference in permafrost distribution may have an important influence on biological activity and decomposition.

Section P-J (Fig. 2, group C) was exposed at a dune field upon Pleistocene gravel and under sparse vegetation cover. Carbon-14 dating of a distinct paleosol obtained a calibrated age of 1.3 ka. IRSL dating from sand provided ages of 0.29 ka above the paleosol and 9.2 to 11.7 ka below the paleosol. The eolian sediment of section P-L (Fig. 2, group B) was located in the valley bottom near the Ider Gol under dense steppe. IRSL dating of eolian sand provided ages of 7.1 and 13.8 ka, whereas ^{14}C dating of SOM and charcoal from paleosols obtained calibrated ages of 8.0 and 9.5 ka.

Sections P-F and P-K (Fig. 2, group A) were located in a valley bottom under dense meadow steppe. A paleo-channel cut into alluvial sediments that were composed of eolian and alluvial layers, paleosols, and humic layers, containing charcoal and small pieces of wood. No permafrost was found, whereas slight deformation of sediment layers indicated former weak cryoturbation. At section P-F, several calibrated

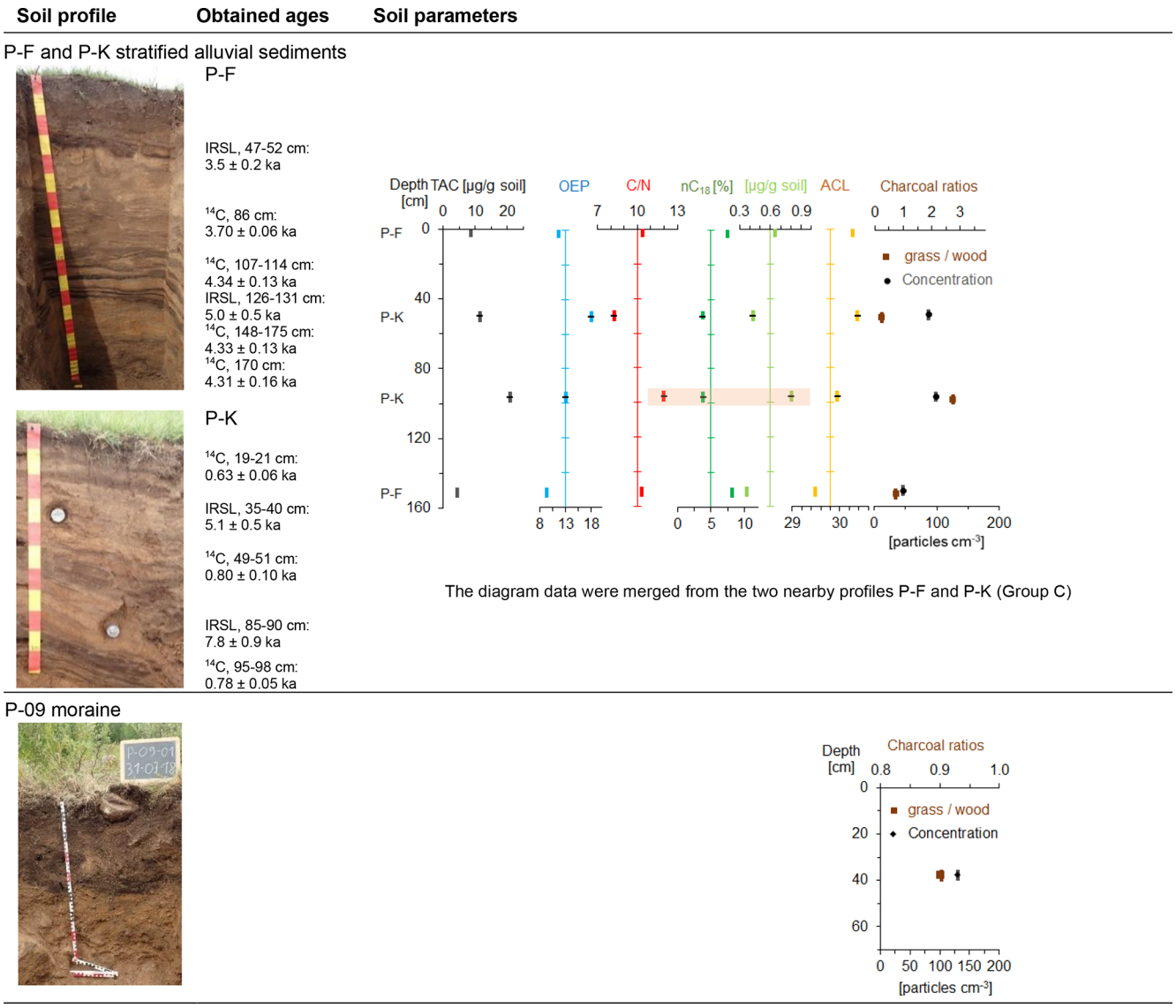

Figure 2.

^{14}C ages of wood and bone artifacts (*Ovis*) provided a consistent chronology between ca. 4.3 and 3.7 ka, which was complemented by two IRSL ages of 3.5 and 5.0 ka. At section P-K, IRSL ages of 5.1 and 7.8 ka were somewhat older compared to section P-F. However, the ^{14}C ages of < 0.8 ka obtained from SOM of three humic layers did not fit into the chronological framework based on the other ages. Contamination by young organic material may have adulterated the dating, and therefore P-K was assigned to group C.

Single samples were taken from three profiles that were not analyzed by radiometric dating. Profile P-M (Fig. 2, group C) was a section in a Pleistocene terrace near a river and was covered by eolian sediments, which contained several cryoturbated paleosols. Profile P-N (Fig. 2, group B) was situated in eolian sand that contained several cryoturbated paleosols above basal moraine. Profile P-09 (Fig. 2, group A) was located at a burned forest site in slope debris above till and contained many charcoals. The paleosol of section P-E (Fig. 2, group A) was developed upon eolian sand and was covered by colluvial sediments. Carbon-14 dating of SOM provided a calibrated age of 12.8 ka. No *n*-alkane analysis was conducted on P-E.

3.2 Macro-charcoal distribution

Macro-charcoal occurred in all samples from paleosols and humic layers. The total amount of macro-charcoal per sample varied between a minimum of 22 and a maximum of 338 particles cm^{-3}, with a mean of 100 particles cm^{-3} (Fig. 3 and Supplement File S1). Charcoal of leaves generally had a lower proportion than charcoal of wood and grass. The ratios

Soil profile	Obtained ages	Soil parameters
Group B: Profiles at steppe sites		
P-C eolian sand and paleosols upon pediment	IRSL, 15-20 cm: 1.1 ± 0.1 ka ^{14}C, 45-50 cm: 0.91 ± 0.07 ka ^{14}C, 65-70 cm: 1.77 ± 0.10 ka IRSL, 70-75 cm: 8.9 ± 0.6 ka IRSL, 128-133 cm: 11.0 ± 1.1 ka	
P-L eolian sand and paleosols in basin	IRSL, 27-32 cm: 7.1 ± 0.5 ka ^{14}C, 56-61 cm: 7.97 ± 0.06 ka ^{14}C, 114-119 cm: 9.53 ± 0.04 ka IRSL, 122-127 cm: 13.8 ± 0.8 ka	
P-N sediment fill in tongue basin of Pleistocene glacier		
P-E slope debris upon eolian sand	IRSL, 77-82 cm: 9.9 ± 0.6 ka ^{14}C, 112 cm: 12.81 ± 0.06 ka IRSL, 180-185 cm: 14.1 ± 1.2 ka IRSL, 218-223 cm: 11.2 ± 1.4 ka IRSL, 250-255 cm: 15.4 ± 1.4 ka IRSL, 290-295 cm: 14.1 ± 1.1 ka	

Figure 2.

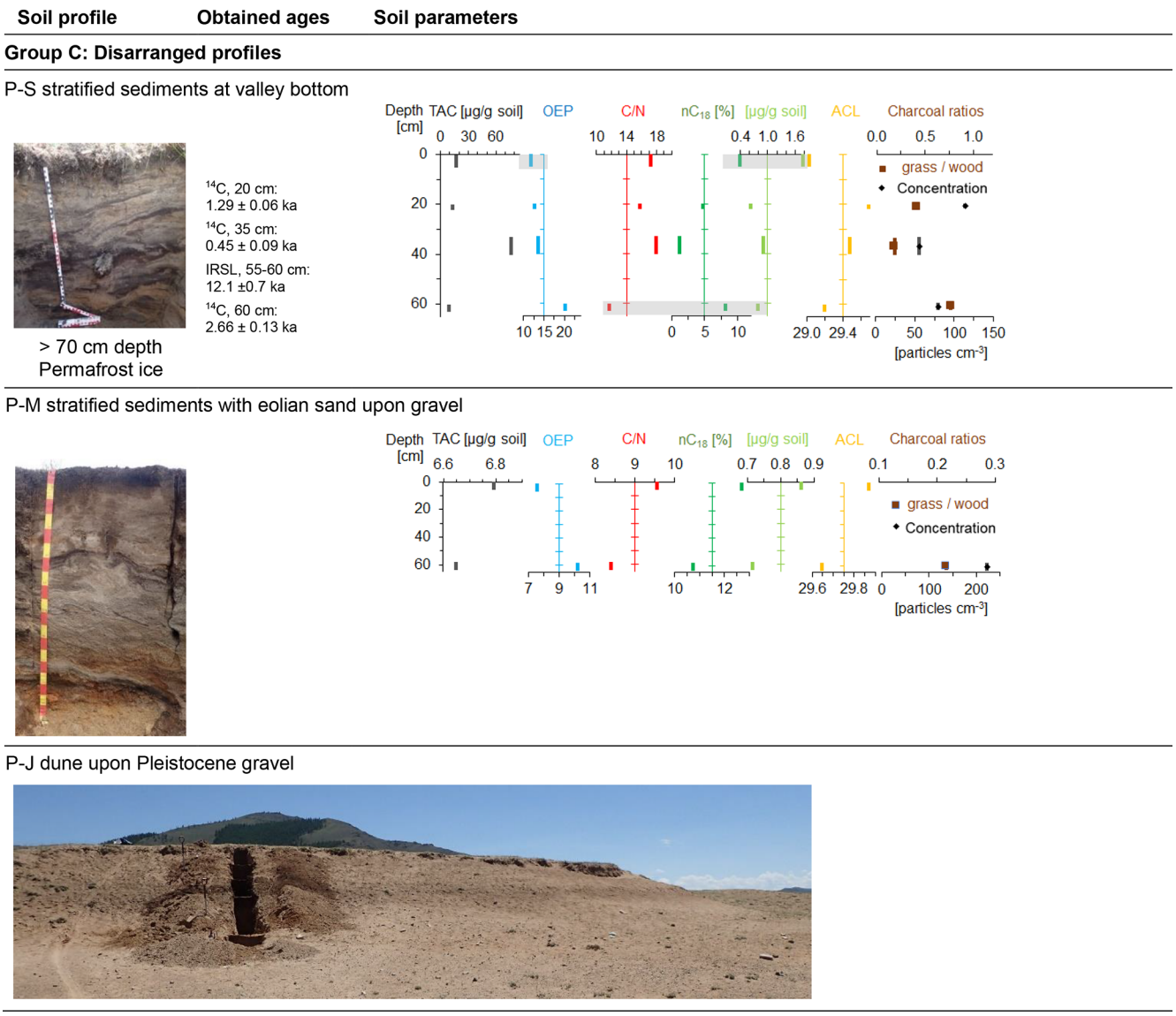

Figure 2. Soil profiles with sampling positions, *n*-alkane and charcoal ratios. Ages for radiometric dating were adapted from Klinge et al. (2022). Grey bars indicate parameters for enhanced biological decomposition, and light brown rectangles indicate parameters for decomposition by fire. Note the different scaling of the horizontal axes.

between charcoal of wood and grass per sample were significantly highly negatively correlated ($r = -0.92$), whereas charcoal of leaves occurred mostly independently from the other two morphotypes (Table 1). The charcoal particle concentration showed no distinct correlation pattern with the site type, sample depth and charcoal type ratio (Fig. 3). At the dune profile P-J, the total amount of charcoal was too low for further interpretations.

Table 1. Correlation coefficient (r) between different charcoal-morphotype distributions ($n = 23$, excluding profile P-J).

Charcoal type	r	p value
Wood–grass	−0.93	< 0.001
Wood–leaf	−0.01	0.969
Grass–leaf	−0.36	0.088

3.3 Patterns of long-chain *n*-alkanes in plants and topsoils

One sample of fresh plant material per species was analyzed for the *n*-alkane distribution from the main species of the study area (Fig. 4). Siberian larch is the dominant tree in the Mongolian forest–steppe, and its *n*-alkane pattern shows dominance in nC_{27} and nC_{29} (Fig. 4), which was also reported by Zech et al. (2010b). In contrast, Struck et al. (2020)

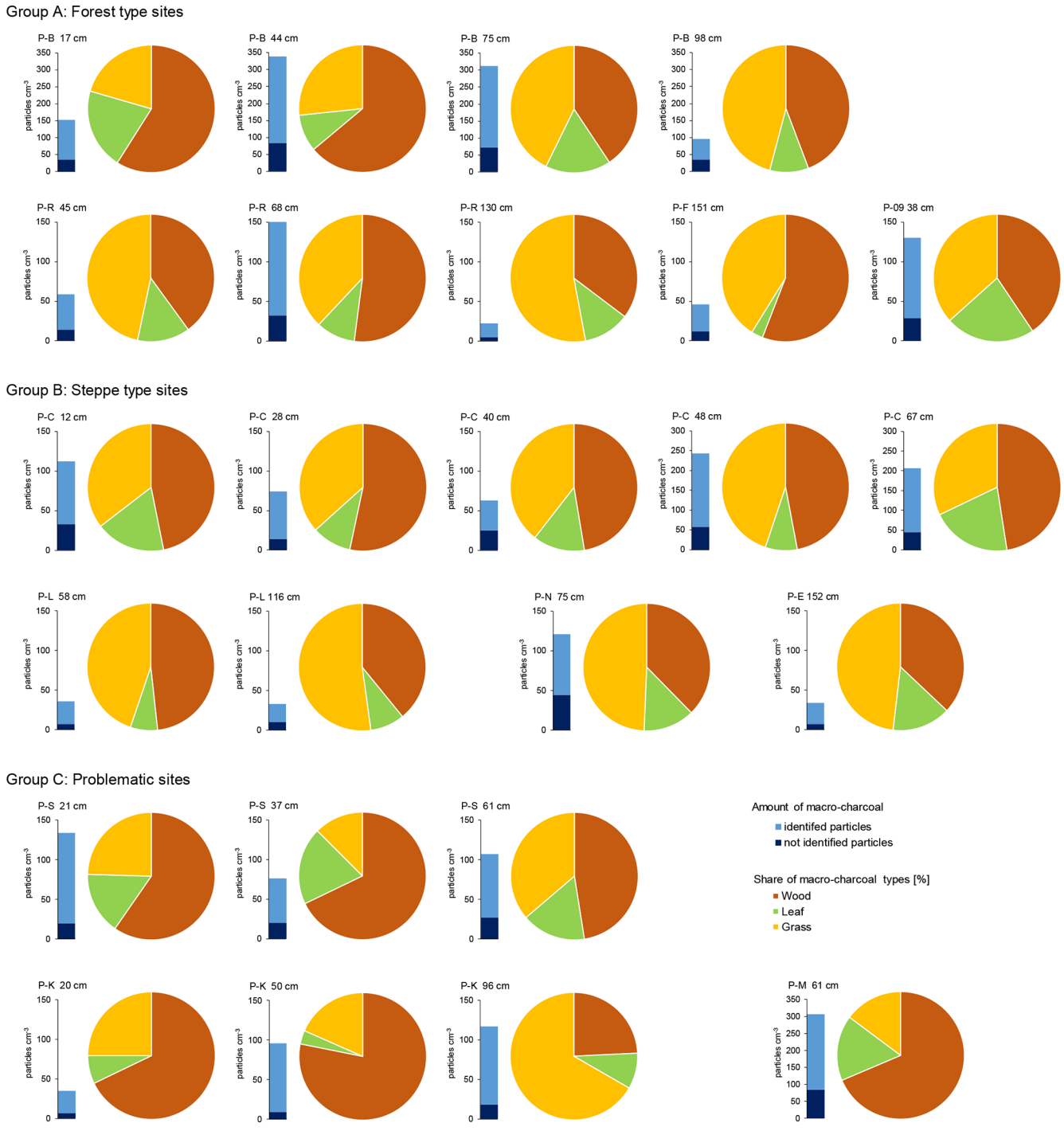

Figure 3. Charcoal concentration and morphotype distribution in paleosols and humic layers at different study sites.

stated a dominance of nC$_{25}$ for their larch samples from Mongolia, whereas Diefendorf et al. (2011) stated a dominance of nC$_{29}$ for *Larix decidua* from North American samples. We detected a low total n-alkane concentration (TAC) of 19.7 µg g^{-1} dry plant material for our Siberian larch sample, which is in agreement with literature data. Thus, larch is unlikely to significantly contribute to the n-alkane patterns of the soils. Birch (*Betula platyphylla*) and willow (*Salix* spp.), which often occur at moist and open sites in forest stands, also have a predominance of nC$_{27}$ and yielded TACs of 248.8 and 96.4 µg g^{-1}, respectively (Fig. 4). Comparable n-alkane distributions with a predominance of nC$_{27}$ for birch species were also reported by Tarasov et al. (2013) (*B. exilis*, *B. fruticosa*) and Zech et al. (2010b) for eastern Siberia and by

Strobel et al. (2021) (*B. nana*) for the Mongolian Altai. Zech et al. (2010b) and Tarasov et al. (2013) also reported a predominance of nC_{27} for willow, whereas the nC_{23} content in our sample was exceptionally high. We assume that moist environmental conditions promote the formation of a higher content of mid-chain *n*-alkanes such as nC_{23} and/or nC_{25} in leaf waxes of willow (Tarasov et al., 2013). *Lonicera altaica*, *Vaccinium vitis-idaea* and *Vaccinium myrtillus* are common shrubs that are restricted to dense pristine forests and thus may serve as secondary indicators for forests. We found a distinct predominance of nC_{29} and high TAC of 493.3 µg g^{-1} for *Lonicera altaica* (Fig. 4), whereas a predominance of nC_{31} was reported for both *Vaccinium vitis-idaea* and *Vaccinium myrtillus* (Tarasov et al., 2013). The authors stated that TAC for *Vaccinium vitis-idaea* was 4070 µg g^{-1} and for *Vaccinium myrtillus* was ∼ 3000 µg g^{-1}.

Poaceae that prevail in the grassland reveal a predominance of nC_{31} and a TAC of 246.6 µg g^{-1} (Fig. 4), which was also shown by Bush and McInerney (2013) and Struck et al. (2020). The same is true for *Potentilla fruticosa*, which represents a dominant forb in the steppe with a TAC of 1200 µg g^{-1} (Fig. 4), as well as for Cyperaceae (Bush and McInerney, 2013; Struck et al., 2020). Furthermore, *Potentilla fruticosa* as a steppe-dominant plant has an increased relative *n*-alkane contribution of nC_{33}. By contrast, *Artemisia* spp., which contribute many prevalent genera of the steppe, as well as *Caragana* spp. have a predominance of nC_{29} (Struck et al., 2020).

Most of the long-chain *n*-alkanes detected in the investigated topsoils show similar patterns with increasing relative contributions of odd *n*-alkanes from nC_{25} to the predominant homologue nC_{31} (Fig. 5), which confirms the results from Schäfer et al. (2016) and Struck et al. (2020). We observed the highest relative abundances of nC_{33} in topsoils of the profiles P-B, P-09 and P-C. This finding can be likely explained with the input of litter from *Potentilla fruticosa*, being characterized by high nC_{33} contents. The OEP ratios of topsoils range between 7.5 and 16.1. A distinct exception of the *n*-alkane pattern in the topsoils occurs at profile P-S. The dominant carbon-chain length for this soil profile is nC_{27} (Fig. 5). Abundant birch and willow trees at this site may have caused this high content of nC_{27}. TAC ranges from 4.5 to 26.7 µg g^{-1} soil and from 107 to 280 µg g^{-1} TOC for the investigated topsoils.

The ACL (Fig. 5) of different topsoils shows marginal relationships to the modern vegetation. Currently, no trees exist at the sites P-C and P-F and dense larch succession occurs at the site P-B. These sites are among those with the highest ACL values in the topsoils. Leaf trees like willow and birch occur in the vicinity of the steppe-dominated sites P-M and P-N and are mixed with larch at the sites P-09, P-R and P-S. Topsoils of P-09 and P-S are characterized by higher content of nC_{27} compared to the other topsoils. The high production rate of nC_{27} of willow and birch produces a distinct signal in the *n*-alkane distribution in topsoil, which decreases the ACL compared to steppe- and larch-dominated sites. Strobel et al. (2021) have shown comparable *n*-alkane patterns in topsoils with nC_{31} predominance at steppe-dominated sites and with nC_{27} predominance at sites with *Betula nana*.

3.4 Correlation of *n*-alkane and macro-charcoal ratios in soil profiles

The correlation between *n*-alkane ACL and charcoal ratios as indicators for steppe and forest distribution of all samples without site classification is low (Table 2), although a common trend in the wood- and grass-dominated share exists ($r > 0.5$).

A detailed statistical analysis considering specific *n*-alkanes and charcoal types (Table 2) has shown that correlations of wood-driven charcoal are significantly positive with nC_{27} and significantly negative with nC_{31} and nC_{33}, whereas these correlations are inverse for grass charcoal. Charcoals from leaves have no significant correlations, which point to the minor relevance of these morphotypes for vegetation reconstruction.

A closer look at *n*-alkane and macro-charcoal ratios shows that grouping the profiles by vegetation pattern and site conditions increases the statistical correlations significantly (Table 3, Fig. 6). In group A, the profiles P-B and P-R are located at forested sites. At profile P-F no trees occur at present, but the analyzed sample at 151 cm depth included fragments of wood alongside charcoal pieces and alluvial forest grows ca. 1 km upstream. Group A shows highly significant correlations between wood, grass, the grass / wood ratio and C / N on the one hand with ACL and OEP on the other hand (Table 3). Increasing OEP and ACL occurred parallel with the increasing share of grass, which is caused by higher contents of long-chain *n*-alkanes (nC_{31}) in grasses than in other plants and is in agreement with results from Struck et al. (2020) and Strobel et al. (2021). In addition, the C / N ratio correlates positively with C_{sf}, OEP and ACL, which indicates less biological decomposition when the portion of grass vegetation increased at forest-related sites. Permafrost distribution in forest stands, which hampers microbial activity, is related to herb and moss ground vegetation, whereas grass inside forest indicates less canopy closure inducing warmer soil conditions.

Group B includes the profiles P-C and P-L, which are located under dry steppe without any trees, and profile P-N occurs under dense meadow steppe in the vicinity of riparian trees. Group B shows generally lower and inverse correlations between charcoal and *n*-alkane ratios compared to group A (Fig. 6, Table 3). In addition, the total quantity of charcoal particles correlates positively with the short- and mid-chain *n*-alkanes nC_{18} and $\sum nC_{17}$–nC_{20}. These *n*-alkane chain lengths can be produced by microbial degradation or in the case of nC_{18} by charring (Wiesenberg et al., 2009; Zech et al., 2010a). The C / N and OEP values do not show significant correlation with charcoal and *n*-alkane ra-

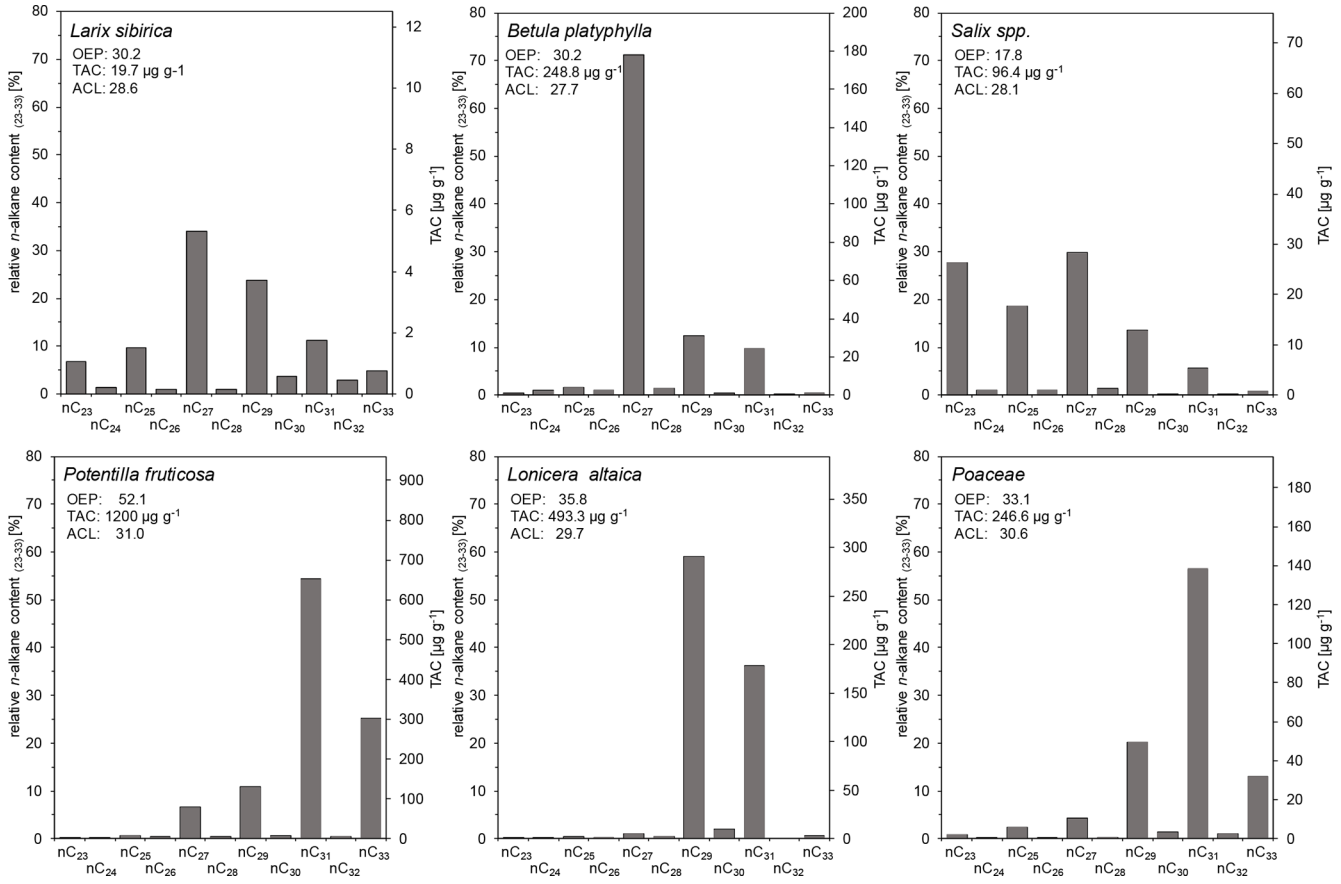

Figure 4. Long-chain n-alkane patterns of plants from the study area at Tosontsengel (OEP, odd-over-even predominance; TAC, total n-alkane concentration of dry plant material; ACL, average chain length of n-alkanes; $n = 1$).

Table 2. Correlation (r) between the relative distribution of charcoal types and ACL (average chain length of n-alkanes, $n = 20$, excluding profile P-K).

Charcoal	nC_{25}	nC_{27}	nC_{29}	nC_{31}	nC_{33}	ACL
Wood	0.20	0.47*	0.23	−0.48*	−0.46*	−0.55*
Leaf	0.03	0.17	−0.08	−0.13	−0.08	−0.17
Grass	−0.18	−0.46*	−0.16	0.45*	0.42	0.53*
Grass / wood (C_{sf})	−0.20	−0.45*	−0.19	0.47*	0.40	0.52*
Grass + leaf / wood	−0.20	−0.44	−0.22	0.48*	0.41	0.51*

* $p < 0.05$.

tios in group B, which may point to less influence of microbial decomposition on these ratios.

Sediment stirring and inverse ages from radiometric dating indicate disturbances and transformations in the organic matter of profiles P-K and P-S, which become visible in the extreme outmost relations between n-alkane and charcoal ratios (Fig. 6). Due to these inconsistencies, these profiles were classified as group C, which is problematic for environmental interpretation.

Figure 2 shows the vertical distribution of charcoal and n-alkane parameters in several soil profiles that were investigated in greater detail. Layers where low values of OEP and C / N and high values of nC_{18} occur are highlighted in grey to indicate the potential of increased microbiological decomposition. Layers where high values of OEP and C / N and nC_{18} occur are highlighted in light brown to indicate the potential of degradation by fire.

The dark-brown-colored humic layers (18–23 cm; 40 cm) of profile P-B show low TAC, OEP and C / N and high nC_{18} and $\sum nC_{17}$–nC_{20} values (Fig. 2), which confirm the assumption of relocated topsoil from an upslope position for these humic layers (Klinge et al., 2021). In contrast,

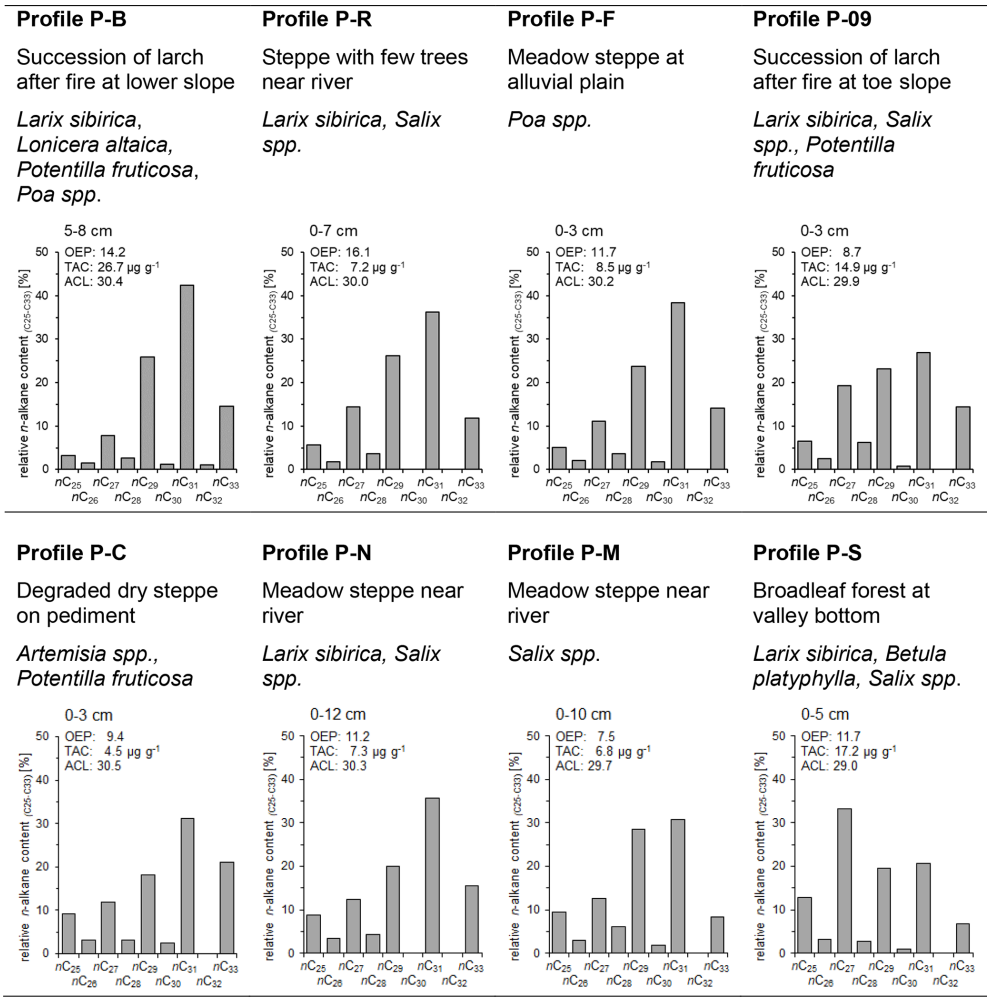

Figure 5. Relative long-chain *n*-alkane content (%), OEP, TAC and ACL of topsoils and mean vegetation at different profiles in the study area (OEP, odd-over-even predominance; TAC, total *n*-alkane concentration of soil; ACL, average chain length of *n*-alkanes).

the bright yellowish sediment (23–38 cm) tends to have increased values for TAC, OEP and C / N and low nC_{18} and $\sum nC_{17}$–nC_{20} values, pointing to more parent material that was subjected to less soil formation. A similar *n*-alkane and C / N pattern occurs in profile P-C, where low OEP and C / N and high nC_{18} of a layer at ∼ 6 cm and a paleosol at 45–50 cm indicated microbiological activity, whereas the other layers were less affected. The inverse distribution of *n*-alkane and macro-charcoal ratios in the pronounced paleosol at 45–50 cm depth in P-C is probably related to the intense decomposition that led to a decrease in long-chain *n*-alkanes and increase in short- and mid-chain *n*-alkanes. The same is true for profile P-L, where the differences in OEP and C / N between the upper layer (58 cm; OEP, 15.6; C / N, 20.1) and lower layer (116 cm; OEP, 9.3; C / N, 14.9) indicate more decomposition related to the decrease in long-chain *n*-alkanes in the latter, which again explains the inverse charcoal ratio (Fig. 2).

At profile P-R, the *n*-alkane pattern is comparable with profile P-B. However, the decomposition rate was already high in the topsoil of profile P-R in contrast to P-B. Although decomposition may have influenced the *n*-alkane pattern of the profiles P-B and P-R, the parallel pattern of macro-charcoal ratios confirms the vegetation proxy. At the top and at the bottom of profile P-F, the OEP, C / N and mid-chain *n*-alkanes indicate similar microbiological activity and soil formation, but ACL points to more forest in the lowest layer.

In the steppe profiles P-C and P-L (group B), higher macro-charcoal ratios that indicate increased grassland share are combined with increased degradation of *n*-alkanes, shown by a lower OEP. This phenomenon is reverse in the forest-related sites (group A, profiles P-B, P-R, P-F). An intensive cryoturbation in profile P-S and substrate infiltration at the profile P-K is underlined by the obtained ages, which diminished the analysis of the *n*-alkane patterns, charcoal ratios and chronology.

Table 3. Correlation matrix between macro-charcoal and *n*-alkane parameters (*r*). TAC denotes total *n*-alkane content; OEP denotes odd-over-even predominance; ACL denotes average chain length of *n*-alkanes.

	nC_{18} (%)	C / N	$\sum nC_{17}$–nC_{20} (%)	TAC	OEP	ACL
Group A: profiles P-B, P-R, P-F; $n = 8$						
Wood	0.18	−0.59	−0.03	−0.40	−0.78*	−0.91**
Leaf	−0.02	−0.51	−0.38	0.23	−0.23	−0.14
Grass	−0.24	−0.37	−0.61	0.27	0.86**	0.93***
Grass / wood; C_{sf}	−0.13	0.85**	−0.28	0.25	0.82*	0.94***
Particles	0.02	−0.55	−0.29	0.35	−0.22	−0.35
C / N	−0.04		−0.11	−0.15	0.59	0.78*
Group B: profiles P-C, P-L, P-N; $n = 8$						
Wood	0.97****	−0.53	0.94***	0.54	0.69	0.83*
Leaf	0.69	−0.43	0.65	−0.10	0.10	0.23
Grass	0.94****	−0.55	0.92**	−0.33	−0.56	−0.75*
Grass / wood; C_{sf}	−0.31	0.19	−0.27	−0.41	−0.66	−0.84**
Particles	0.96****	−0.55	0.93***	0.06	−0.46	−0.17
C / N	−0.45		−0.34	−0.59	0.38	0.13
	Macro-charcoal particle quantity			Macro-charcoal particle proportion		

* $p < 0.05$. ** $p < 0.01$. *** $p < 0.001$. **** $p < 0.0005$.

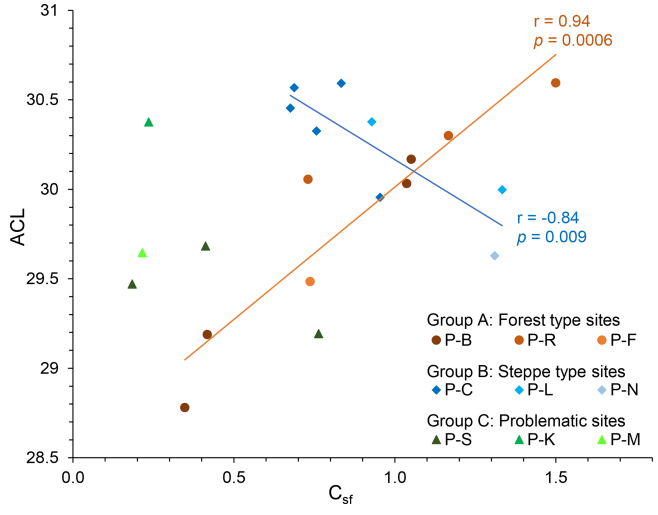

Figure 6. Linear regressions between ACL and C_{sf} grouped by different site conditions (ACL, average chain length of *n*-alkanes; C_{sf}, macro-charcoal grass / wood ratio).

3.5 Evaluating the impact of geomorphological processes, climate and vegetation on *n*-alkanes and macro-charcoal distribution in soils for their suitability as proxy data

The horizontal distribution of *n*-alkane and macro-charcoal ratios in different profiles show parallel patterns in group A and inverse patterns in group B (Fig. 2). A distinct environmental difference between both groups is the occurrence of modern or past forest at the sites of group A, whereas forest was probably absent at the sites of group B. Positive correlations between both ratios may prove the delineation of paleovegetation at the specific sample sites, whereas diverging ratios derive from different sources, pathways and degradation degrees of elements. Irregular biomarker and charcoal distributions in disturbed profiles show inconsistent dating results too, which clearly points to problematic samples that should be interpreted with caution or rejected.

Most of the *n*-alkanes in topsoils originate directly from the litter of the covering vegetation. A paleosol most likely received *n*-alkanes that indicate the local vegetation composition, whereas distinct humic layers as deposits of translocated paleosol contain SOM that comes from distant positions. Thus, *n*-alkanes of colluvial layers represent a mixture of solum material from the upslope area, whereas alluvial layers may receive additional organic material from a larger area of the fluvial catchment. Furthermore, reworked leaf waxes and fossil *n*-alkanes may have deposited along with eolian influx and may have biased the biomarker signals (Haas et al., 2017). However, it can be presumed that the eolian portion of *n*-alkanes in soils is negligible compared to those directly deriving from vegetation.

Paleosols and humic layers contain organic carbon from different sources such as reworked solum material, charcoal, plant material, living roots and dissolved organic matter, which produces uncertainties of > 100 years by ^{14}C dating (Pessenda et al., 2001). Carbon-14 dating of charcoal pro-

vides the age of tree growth before fire. Carbon-14 dating on *n*-alkanes reflects the age of modern vegetation or paleovegetation (i.e., *n*-alkane-producing vegetation) and its input into soils. Therefore, we decided to focus the age determination of our soils using ^{14}C and IRSL dating on bulk material. The *n*-alkane assemblage in the SOM covers the entire period of soil development. Although soil formation may last for a long time, when no soil erosion or sediment covering occurred, the high age frequency of humic layers and paleosols found in our soil profiles (Fig. 2) limits most of the soil formation periods to a few hundred years.

n-Alkanes are subjected to microbiological degradation, which is controlled by different ecological factors relating to moisture and temperature regimes in the investigated soils (Struck et al., 2020). Our results have shown that decomposition of organic matter was generally higher in dry steppe soils and lower under forest that is often underlain by permafrost. The degradation of *n*-alkanes in Mongolian topsoils from semi-arid and arid regions was also investigated for two transects by Struck et al. (2020). OEP values for these topsoils range from 1.5 to 19 and agree with our OEP results (Struck et al., 2020) (Fig. 5).

Although small pieces of charred wood were found in many profiles, the "macro-charcoals" that were analyzed here are particles of microscopic size in the scope of pollen and dust. Thus, macro-charcoals of local origin and eolian input were deposited in different shares. Increasing particle concentration may serve as an indicator for a macro-charcoal source of nearer rather than long-distance fire. Treeless sites of the steppe area (profiles P-C, P-L) must have received their wood-derived macro-charcoal portion in particular by eolian influx. In contrast, the *n*-alkane patterns of steppe soils represent the local vegetation cover consisting of grasses and herbs. The increased share of short- and mid-chain *n*-alkanes (nC_{18}–nC_{26}) in combination with a decreased OEP ratio suggests a more intense microbial degradation of *n*-alkanes (Lerch et al., 2018). Furthermore, statistical analysis (Table 3) proved that a combination of macro-charcoal and *n*-alkanes yields inconsistent results for steppe soils (group B).

The information of macro-charcoal and *n*-alkane distribution (ACL) and the dating results from the paleosols and humic layers provide a chronological framework of the Holocene vegetation evolution in the study area (Fig. 7). Both indices show that grassland dominated in the period before 7.5 ka, although forests had already existed in the Khangai Mountains since at least 9.5 ka (Gunin et al., 1999; Wang et al., 2009; Unkelbach et al., 2021). After 5.0 ka, the indices are more diverse and the vegetation pattern becomes more complex. The site-specific *n*-alkane proxy tends to indicate more grassland compared to the macro-charcoal proxy, which was probably influenced by eolian deposition of allochthonous charcoal particles upon topsoils. The widespread dispersal of charcoal particles after forest and steppe fires represents a distinct sedimentation factor that can even be traced to the high mountains as dust in glacier ice

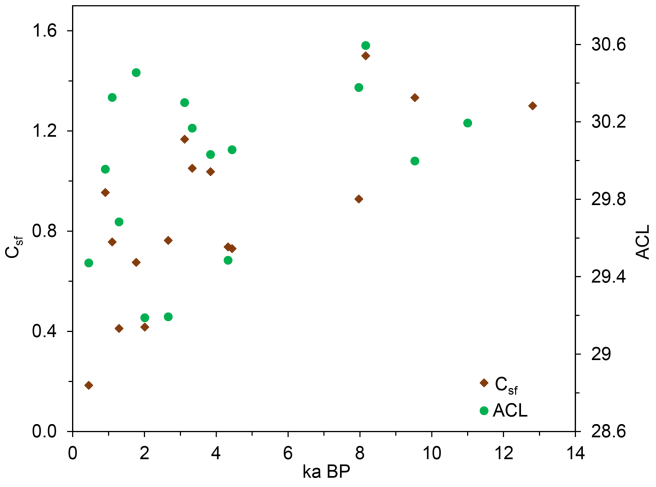

Figure 7. Chronological distribution of macro-charcoal ratio and ACL (ACL, average chain length of *n*-alkanes; C_{sf}, macro-charcoal grass / wood ratio).

(Eichler et al., 2011; Brugger et al., 2018). Thus, the higher share of wood-derived macro-charcoal in soils points to increased forest fires in the region. In addition, the *n*-alkane patterns that represent more local proxies in soils indicate an expanded steppe area for most of the soil profiles, established by a high content of nC_{31}, since the beginning of the Late Holocene. The observed change in the pattern of forest and steppe distribution as well as the increased fire activity in Mongolia since the Late Holocene is related to climatic and/or anthropogenic impact (Klinge and Sauer, 2019). Furthermore, desertification processes and increased geomorphological activity occur concordantly with a cultural change since the early Bronze Age when humans developed a pastoral economy (Fernández-Giménez et al., 2017; Klinge et al., 2022). Nevertheless, these initial findings need further evaluation due to the limited number of samples presented here.

4 Conclusions

Based on our results of comparing two different paleoproxies, *n*-alkanes and macro-charcoals, we have shown that it is essential to consider their different element sources, paths and catchment areas for interpretation of the local and regional paleo-environment. Additional information about soil properties as well as radiometric dating provides further evidence. The analysis of lipid biomarkers, such as *n*-alkanes, on samples from soil profiles of central Mongolia gives insight into local vegetation conditions. *n*-Alkanes, which are organic molecules in leaf waxes, are directly accumulated in the soils by local vegetation (Zech et al., 2010b). Translocation of soil material may occur by slope wash and solifluction processes. Decomposition of organic matter and *n*-alkanes is generally more intense in dry steppe soils and

less intense under forest that is often underlain by permafrost. Macro-charcoals in soils represent a mixture of both local and long-distance sources. Due to the eolian transport, the dominating wind direction frames the catchment area of macro-charcoal influx.

We have shown that paleosols and humic layers represent a valuable archive for reconstruction of the detailed paleo-environment at a high site-specific spatial resolution. The application of lipid biomarker analysis to paleosols can help to prove local differences in topographic site conditions over time such as the aspect-dependent vegetation differentiation of the Mongolian forest–steppe. Charcoal in paleosols indicates periods of increased fire impact on landscape evolution and geomorphology. However, the temporal resolution of paleosol and sediment archives is often low and discontinuous due to irregular deposition intensity and soil-forming periods, but the biomarker proxies are related to distinct geomorphological periods in a local scale. In contrast, lake sediments may provide a more continuous sedimentation chronology, but the sediment input depends on fluvial and eolian catchments. Thus, these archives contain proxy data that represent a larger area than soil archives do. Furthermore, stratified charcoal particles in glacier ice and snow fields solely derive from long-distance eolian transport. Their paleo-proxies depend on the main wind direction that frames the catchment area and thus the region for the paleo-environmental representation of their proxies. In summary, there is further need for multi-proxy analysis (biomarkers, macro-charcoal, pollen, microorganisms, ancient DNA, sediment properties) comparing the different soils, lake and glacier archives in combination with radiometric dating to enhance and refine the paleo-environmental records in Mongolia.

Data availability. All raw data can be provided by the corresponding authors upon request.

Supplement. The supplement related to this article is available online at: https://doi.org/10.5194/egqsj-71-91-2022-supplement.

Author contributions. FS and ML developed the project idea in collaboration with MK and JU. Fieldwork was carried out by FS and MK. ML and JU carried out most of the laboratory work. MK analyzed the data. MK prepared the manuscript, and ML, JU, MZ and FS contributed to the discussion of the results and read and approved the manuscript.

Competing interests. At least one of the (co-)authors is a member of the editorial board of *E&G Quaternary Science Journal*. The peer-review process was guided by an independent editor, and the authors have also no other competing interests to declare.

Disclaimer. Publisher's note: Copernicus Publications remains neutral with regard to jurisdictional claims in published maps and institutional affiliations.

Acknowledgements. We thank our project partners Choimaa Dulamsuren and Markus Hauck (Faculty of Environment and Natural Resources, University of Freiburg) and Uudus Bayarsaikhan (Department of Biology, National University of Mongolia, Ulaanbaatar) for their great support during the fieldwork in Mongolia.

We thank Daramragchaa Tuya (Tarvagatai Nuruu National Park, Tosontsengel Sum, Zavkhan Aimag, Mongolia) for her invaluable support of our research. We wish to express our gratitude to our Mongolian colleagues Amarbayasgalan, Enkhjargal and Enkh-Agar. We greatly appreciated their hospitality and help in the field. Our thanks also go to the German students Jannik Brodthuhn and Tim Rollwage for their assistance during soil sampling in Mongolia.

In particular, we thank Daniela Sauer (Institute of Geography, University of Göttingen) and Manfred Frechen (Leibniz Institute for Applied Geophysics, Hanover) for their professional support and project collaboration. Furthermore, we thank Bruno Glaser and Tobias Bromm (Department of Soil Biogeochemistry, Martin Luther University Halle-Wittenberg) for providing access to laboratory facilities and support of laboratory analyses. We thank Hermann Behling (Albrecht-von-Haller-Institute for Plant Sciences, University of Göttingen) for providing laboratory access.

We also thank Jens Holtvoeth and the anonymous reviewer for their valuable recommendations to improve the manuscript.

Financial support. This research has been supported by the Deutsche Forschungsgemeinschaft (grant no. 385460422).

This open-access publication was funded
by the University of Göttingen.

Review statement. This paper was edited by Ingmar Unkel and reviewed by Jens Holtvoeth and one anonymous referee.

References

Academy of Sciences of Mongolia and Academy of Sciences of USSR: National Atlas of the Peoples Republic of Mongolia, Ulan Baatar, Moscow, 144 pp., 1990.

Bittner, L., Bliedtner, M., Grady, D., Gil-Romera, G., Martin-Jones, C., Lemma, B., Mekonnen, B., Lamb, H. F., Yang, H., Glaser, B., Szidat, S., Salazar, G., Rose, N. L., Opgenoorth, L., Miehe, G., Zech, W., and Zech, M.: Revisiting afro-alpine Lake Garba Guracha in the Bale Mountains of Ethiopia: rationale, chronology, geochemistry, and paleoenvironmental implications, J. Paleolimnol., 64, 293–314, https://doi.org/10.1007/s10933-020-00138-w, 2020.

Bliedtner, M., Schäfer, I. K., Zech, R., and von Suchodoletz, H.: Leaf wax *n*-alkanes in modern plants and topsoils from eastern Georgia (Caucasus) – implications for reconstruct-

ing regional paleovegetation, Biogeosciences, 15, 3927–3936, https://doi.org/10.5194/bg-15-3927-2018, 2018.

Bliedtner, M., von Suchodoletz, H., Schäfer, I., Welte, C., Salazar, G., Szidat, S., Haas, M., Dubois, N., and Zech, R.: Age and origin of leaf wax *n*-alkanes in fluvial sediment–paleosol sequences and implications for paleoenvironmental reconstructions, Hydrol. Earth Syst. Sci., 24, 2105–2120, https://doi.org/10.5194/hess-24-2105-2020, 2020.

Breckle, S.-W., Lawlor, G., Lawlor, D. W., and Walter, H. (Eds.): Walter's vegetation of the earth: The ecological systems of the geo-biosphere, 4th edn., Springer, Berlin, 527 pp., ISBN 9783540433156, 2002.

Brugger, S. O., Gobet, E., Sigl, M., Osmont, D., Papina, T., Rudaya, N., Schwikowski, M., and Tinner, W.: Ice records provide new insights into climatic vulnerability of Central Asian forest and steppe communities, Global Planet. Change, 169, 188–201, https://doi.org/10.1016/j.gloplacha.2018.07.010, 2018.

Buggle, B., Wiesenberg, G. L., and Glaser, B.: Is there a possibility to correct fossil *n*-alkane data for postsedimentary alteration effects?, Appl. Geochem., 25, 947–957, https://doi.org/10.1016/j.apgeochem.2010.04.003, 2010.

Bush, R. T. and McInerney, F. A.: Leaf wax *n*-alkane distributions in and across modern plants: Implications for paleoecology and chemotaxonomy, Geochim. Cosmochim. Ac., 117, 161–179, https://doi.org/10.1016/j.gca.2013.04.016, 2013.

Diefendorf, A. F., Freeman, K. H., Wing, S. L., and Graham, H. V.: Production of *n*-alkyl lipids in living plants and implications for the geologic past, Geochim. Cosmochim. Ac., 75, 7472–7485, https://doi.org/10.1016/j.gca.2011.09.028, 2011.

Dulamsuren, C. and Hauck, M.: Spatial and seasonal variation of climate on steppe slopes of the northern Mongolian mountain taiga, Grassl. Sci., 54, 217–230, https://doi.org/10.1111/j.1744-697X.2008.00128.x, 2008.

Eglinton, G. and Hamilton, R. J.: Leaf epicuticular waxes, Science, 1322–1325, 1967.

Eichler, A., Tinner, W., Brütsch, S., Olivier, S., Papina, T., and Schwikowski, M.: An ice-core based history of Siberian forest fires since AD 1250, Quaternary Sci. Rev., 30, 1027–1034, https://doi.org/10.1016/j.quascirev.2011.02.007, 2011.

Erdős, L., Ambarlı, D., Anenkhonov, O. A., Bátori, Z., Cserhalmi, D., Kiss, M., Kröel-Dulay, G., Liu, H., Magnes, M., Molnár, Z., Naqinezhad, A., Semenishchenkov, Y. A., Tölgyesi, C., and Török, P.: The edge of two worlds: A new review and synthesis on Eurasian forest-steppes, Appl. Veg. Sci., 21, 345–362, https://doi.org/10.1111/avsc.12382, 2018.

Fernández-Giménez, M. E., Venable, N. H., Angerer, J., Fassnacht, S. R., Reid, R. S., and Khishigbayar, J.: Exploring linked ecological and cultural tipping points in Mongolia, Anthropocene, 17, 46–69, https://doi.org/10.1016/j.ancene.2017.01.003, 2017.

Fowell, S. J., Hansen, B. C., Peck, J. A., Khosbayar, P., and Ganbold, E.: Mid to late Holocene climate evolution of the Lake Telmen Basin, North Central Mongolia, based on palynological data, Quat. Res., 59, 353–363, https://doi.org/10.1016/S0033-5894(02)00020-0, 2003.

Gunin, P. D., Vastokova, E. A., Dorofeyuj, N. I., Tarasov, P. E., and Black, C. C. (Eds.): Vegetation dynamics of Mongolia, Geobotany, 26, Kluwer Academic Publishers, Dordrecht, Boston, London, 238 pp., https://doi.org/10.1007/978-94-015-9143-0_2, 1999.

Haas, M., Bliedtner, M., Borodynkin, I., Salazar, G., Szidat, S., Eglinton, T. I., and Zech, R.: Radiocarbon Dating of Leaf Waxes in the Loess-Paleosol Sequence Kurtak, Central Siberia, Radiocarbon, 59, 165–176, https://doi.org/10.1017/RDC.2017.1, 2017.

Hais, M., Chytrý, M., and Horsák, M.: Exposure-related forest-steppe: A diverse landscape type determined by topography and climate, J. Arid Environ., 135, 75–84, https://doi.org/10.1016/j.jaridenv.2016.08.011, 2016.

Hepp, J., Zech, R., Rozanski, K., Tuthorn, M., Glaser, B., Greule, M., Keppler, F., Huang, Y., Zech, W., and Zech, M.: Late Quaternary relative humidity changes from Mt. Kilimanjaro, based on a coupled 2H-18O biomarker paleohygrometer approach, Quatern. Int., 438, 116–130, https://doi.org/10.1016/j.quaint.2017.03.059, 2017.

Hessl, A. E., Brown, P., Byambasuren, O., Cockrell, S., Leland, C., Cook, E., Nachin, B., Pederson, N., Saladyga, T., and Suran, B.: Fire and climate in Mongolia (1532–2010 Common Era), Geophys. Res. Lett., 43, 6519–6527, https://doi.org/10.1002/2016GL069059, 2016.

Hoefs, M. J., Rijpstra, W. C., and Sinninghe Damsté, J. S.: The influence of oxic degradation on the sedimentary biomarker record I: evidence from Madeira Abyssal Plain turbidites, Geochim. Cosmochim. Ac., 66, 2719–2735, https://doi.org/10.1016/S0016-7037(02)00864-5, 2002.

Iijima, Y., Ishikawa, M., and Jambaljav, Y.: Hydrological cycle in relation to permafrost environment in forest-grassland ecotone in Mongolia, Journal of Japanese Association of Hydrological Sciences, 42, 119–130, 2012.

Khansaritoreh, E., Dulamsuren, C., Klinge, M., Ariunbaatar, T., Bat-Enerel, B., Batsaikhan, G., Ganbaatar, K., Saindovdon, D., Yeruult, Y., Tsogtbaatar, J., Tuya, D., Leuschner, C., and Hauck, M.: Higher climate warming sensitivity of Siberian larch in small than large forest islands in the fragmented Mongolian forest steppe, Glob. Change Biol., 23, 3675–3689, https://doi.org/10.1111/gcb.13750, 2017.

Khapugin, A. A., Vargot, E. V., and Chugunov, G. G.: Vegetation recovery in fire-damaged forests: a case study at the southern boundary of the taiga zone, Forestry Studies, 64, 39–50, https://doi.org/10.1515/fsmu-2016-0003, 2016.

Klinge, M. and Sauer, D.: Spatial pattern of Late Glacial and Holocene climatic and environmental development in Western Mongolia – A critical review and synthesis, Quaternary Sci. Rev., 210, 26–50, https://doi.org/10.1016/j.quascirev.2019.02.020, 2019.

Klinge, M., Dulamsuren, C., Erasmi, S., Karger, D. N., and Hauck, M.: Climate effects on vegetation vitality at the treeline of boreal forests of Mongolia, Biogeosciences, 15, 1319–1333, https://doi.org/10.5194/bg-15-1319-2018, 2018.

Klinge, M., Schneider, F., Dulamsuren, C., Arndt, K., Bayarsaikhan, U., and Sauer, D.: Interrelations between vegetation, natural and anthropogenic disturbances, and discontinuous permafrost in the forest-steppe of central Mongolia, Earth Surf. Proc. Land., 46, 1766–1782, https://doi.org/10.1002/esp.5116, 2021.

Klinge, M., Schneider, F., Yan, L., Frechen, M., and Sauer, D.: Alternating geomorphological processes in the northern Khangai Mountains, Mongolia since the Late Glacial period, Geomorphology, 401, 108113, https://doi.org/10.1016/j.geomorph.2022.108113, 2022.

Kolattukudy, P. E.: Biochemistry of plant waxes, in: Chemistry and biochemistry of natural waxes, edited by: Kolattukudy, P. E. and Kolattukudy, P. E., Elsevier, Amsterdam, 290–349, ISBN 0444414703, 1976.

Kopp, B. J., Minderlein, S., and Menzel, L.: Soil Moisture Dynamics in a Mountainous Headwater Area in the Discontinuous Permafrost Zone of northern Mongolia, Arct. Antarct. Alp. Res., 46, 459–470, https://doi.org/10.1657/1938-4246-46.2.459, 2014.

Lerch, M., Bliedtner, M., Roettig, C.-B., Schmidt, J.-U., Szidat, S., Salazar, G., Zech, R., Glaser, B., Kleber, A., and Zech, M.: Lipid biomarkers in aeolian sediments under desert pavements – potential and first results from the Black Rock Desert, Utah, USA, and Fuerteventura, Canary Islands, Spain, E&G Quaternary Sci. J., 66, 103–108, https://doi.org/10.5194/egqsj-66-103-2018, 2018.

Miehe, G., Schlütz, F., Miehe, S., Opgenoorth, L., Cermak, J., Samiya, R., Jäger, E. J., and Wesche, K.: Mountain forest islands and Holocene environmental changes in Central Asia: A case study from the southern Gobi Altay, Mongolia, Palaeogeogr. Palaeoclimatol. Palaeoecol., 250, 150–166, https://doi.org/10.1016/j.palaeo.2007.03.022, 2007.

Mustaphi, C. J. C. and Pisaric, M. F.: A classification for macroscopic charcoal morphologies found in Holocene lacustrine sediments, Prog. Phys. Geog., 38, 734–754, https://doi.org/10.1177/0309133314548886, 2014.

Nyamjav, B., Goldammer, G., and Uibrig, H.: Fire situation in Mongolia, in: International Forest Fire News, 46–66, 2007.

Odgaard, B. V.: Fossil pollen as a record of past biodiversity, J. Biogeogr., 26, 7–17, https://doi.org/10.1046/j.1365-2699.1999.00280.x, 1999.

Patterson, W. A., Edwards, K. J., and Maguire, D. J.: Microscopic charcoal as a fossil indicator of fire, Quaternary Sci. Rev., 6, 3–23, https://doi.org/10.1016/0277-3791(87)90012-6, 1987.

Pelletier, J. D., Barron-Gafford, G. A., Gutiérrez-Jurado, H., Hinckley, E.-L. S., Istanbulluoglu, E., McGuire, L. A., Niu, G.-Y., Poulos, M. J., Rasmussen, C., Richardson, P., Swetnam, T. L., and Tucker, G. E.: Which way do you lean? Using slope aspect variations to understand Critical Zone processes and feedbacks, Earth Surf. Proc. Land., 43, 1133–1154, https://doi.org/10.1002/esp.4306, 2018.

Pessenda, L. C. R., Gouveia, S. E. M., and Aravena, R.: Radiocarbon Dating of Total Soil Organic Matter and Humin Fraction and Its Comparison with ^{14}C Ages of Fossil Charcoal, Radiocarbon, 43, 595–601, https://doi.org/10.1017/S0033822200041242, 2001.

Poynter, J. G., Farrimond, P., Robinson, N., and Eglinton, G.: Aeolian-Derived Higher Plant Lipids in the Marine Sedimentary Record: Links with Palaeoclimate, in: Paleoclimatology and Paleometeorology: Modern and Past Patterns of Global Atmospheric Transport, edited by: Leinen, M. and Sarnthein, M., Springer, Dordrecht, 435–462, https://doi.org/10.1007/978-94-009-0995-3_18, 1989.

Rudaya, N., Tarasov, P. E., Dorofeyuk, N., Solovieva, N., Kalugin, I., Andreev, A., Daryin, A., Diekmann, B., Riedel, F., and Tserendash, N.: Holocene environments and climate in the Mongolian Altai reconstructed from the Hoton-Nur pollen and diatom records: A step towards better understanding climate dynamics in Central Asia, Quaternary Sci. Rev., 28, 540–554, https://doi.org/10.1016/j.quascirev.2008.10.013, 2009.

Schäfer, I. K., Lanny, V., Franke, J., Eglinton, T. I., Zech, M., Vysloužilová, B., and Zech, R.: Leaf waxes in litter and topsoils along a European transect, SOIL, 2, 551–564, https://doi.org/10.5194/soil-2-551-2016, 2016.

Schneider, F., Klinge, M., Brodthuhn, J., Peplau, T., and Sauer, D.: Hydrological soil properties control tree regrowth after forest disturbance in the forest steppe of central Mongolia, SOIL, 7, 563–584, https://doi.org/10.5194/soil-7-563-2021, 2021.

Stevenson, J. and Haberle, S.: Macro Charcoal Analysis: A modified technique used by the Department of Archaeology and Natural History, Palaeoworks Technical Papers, 5, http://hdl.handle.net/1885/144170 (last access: 20 May 2022), 2005.

Strobel, P., Struck, J., Zech, R., and Bliedtner, M.: The spatial distribution of sedimentary compounds and their environmental implications in surface sediments of Lake Khar Nuur (Mongolian Altai), Earth Surf. Proc. Land., 46, 611–625, https://doi.org/10.1002/esp.5049, 2021.

Struck, J., Roettig, C. B., Faust, D., and Zech, R.: Leaf waxes from aeolianite–paleosol sequences on Fuerteventura and their potential for paleoenvironmental and climate reconstructions in the arid subtropics, E&G Quaternary Sci. J., 66, 109–114, https://doi.org/10.5194/egqsj-66-109-2018, 2018.

Struck, J., Bliedtner, M., Strobel, P., Schumacher, J., Bazarradnaa, E., and Zech, R.: Leaf wax n-alkane patterns and compound-specific δ^{13}C of plants and topsoils from semi-arid and arid Mongolia, Biogeosciences, 17, 567–580, https://doi.org/10.5194/bg-17-567-2020, 2020.

Tarasov, P. E., Müller, S., Zech, M., Andreeva, D., Diekmann, B., and Leipe, C.: Last glacial vegetation reconstructions in the extreme-continental eastern Asia: Potentials of pollen and n-alkane biomarker analyses, Quatern. Int., 290–291, 253–263, https://doi.org/10.1016/j.quaint.2012.04.007, 2013.

Thomas, C. L., Jansen, B., van Loon, E. E., and Wiesenberg, G. L. B.: Transformation of n-alkanes from plant to soil: a review, SOIL, 7, 785–809, https://doi.org/10.5194/soil-7-785-2021, 2021.

Umbanhowar, C. E. and Mcgrath, M. J.: Experimental production and analysis of microscopic charcoal from wood, leaves and grasses, Holocene, 8, 341–346, https://doi.org/10.1191/095968398666496051, 1998.

Umbanhowar, C. E., Shinneman, A. L., Tserenkhand, G., Hammon, E. R., Lor, P., and Nail, K.: Regional fire history based on charcoal analysis of sediments from nine lakes in western Mongolia, Holocene, 19, 611–624, https://doi.org/10.1177/0959683609104039, 2009.

Unkelbach, J., Kashima, K., Enters, D., Dulamsuren, C., Punsalpaamuu, G., and Behling, H.: Late Holocene (Meghalayan) palaeoenvironmental evolution inferred from multi-proxy-studies of lacustrine sediments from the Dayan Nuur region of Mongolia, Palaeogeogr. Palaeoclimatol. Palaeoecol., 530, 1–14, https://doi.org/10.1016/j.palaeo.2019.05.021, 2019.

Unkelbach, J., Dulamsuren, C., Klinge, M., and Behling, H.: Holocene high-resolution forest-steppe and environmental dynamics in the Tarvagatai Mountains, north-central Mongolia, over the last 9570 cal yr BP, Quaternary Sci. Rev., 266, 107076, https://doi.org/10.1016/j.quascirev.2021.107076, 2021.

Wang, W., Ma, Y., Feng, Z.-D., Meng, H., Sang, Y., and Zhai, X.: Vegetation and climate changes during the last 8660 cal. a BP in central Mongolia, based on a high resolution pollen

record from Lake Ugii Nuur, Chinese Sci. Bull., 54, 1579–1589, https://doi.org/10.1007/s11434-009-0023-8, 2009.

Wiesenberg, G., Lehndorff, E., and Schwark, L.: Thermal degradation of rye and maize straw: Lipid pattern changes as a function of temperature, Org. Geochem., 40, 167–174, https://doi.org/10.1016/j.orggeochem.2008.11.004, 2009.

Zech, M., Buggle, B., Leiber, K., Marković, S., Glaser, B., Hambach, U., Huwe, B., Stevens, T., Sümegi, P., Wiesenberg, G., and Zöller, L.: Reconstructing Quaternary vegetation history in the Carpathian Basin, SE-Europe, using *n*-alkane biomarkers as molecular fossils: Problems and possible solutions, potential and limitations, E&G Quaternary Sci. J., 58, 148–155, https://doi.org/10.3285/eg.58.2.03, 2010a.

Zech, M., Andreev, A., Zech, R., Müller, S., Hambach, U., Frechen, M., and Zech, W.: Quaternary vegetation changes derived from a loess-like permafrost palaeosol sequence in northeast Siberia using alkane biomarker and pollen analyses, Boreas, 4142, 540–550, https://doi.org/10.1111/j.1502-3885.2009.00132.x, 2010b.

Zech, M., Rass, S., Buggle, B., Löscher, M., and Zöller, L.: Reconstruction of the late Quaternary paleoenvironments of the Nussloch loess paleosol sequence, Germany, using *n*-alkane biomarkers, Quat. Res., 78, 226–235, https://doi.org/10.1016/j.yqres.2012.05.006, 2012.

Zech, M., Krause, T., Meszner, S., and Faust, D.: Incorrect when uncorrected: Reconstructing vegetation history using *n*-alkane biomarkers in loess-paleosol sequences – A case study from the Saxonian loess region, Germany, Quatern. Int., 296, 108–116, https://doi.org/10.1016/j.quaint.2012.01.023, 2013.

Zech, M., Kreutzer, S., Zech, R., Goslar, T., Meszner, S., McIntyre, C., Häggi, C., Eglinton, T., Faust, D., and Fuchs, M.: Comparative ^{14}C and OSL dating of loess-paleosol sequences to evaluate post-depositional contamination of *n*-alkane biomarkers, Quat. Res., 87, 180–189, https://doi.org/10.1017/qua.2016.7, 2017.